Smart Structures and Systems, *Vol. 28, No. 2 (2021) 245-259*
https://doi.org/10.12989/sss.2021.28.2.245

An inerter-system chain and energy-based optimal control of adjacent single-degree-of-freedom structures

Qingjun Chen [1,2], Zhipeng Zhao*[1,2] and Ruifu Zhang [1,2]

[1] *State Key Laboratory of Disaster Reduction in Civil Engineering, Tongji University, Shanghai 200092, China*
[2] *Department of Disaster Mitigation for Structures, Tongji University, Shanghai 200092, China*

(*Received July 5, 2020, Revised October 21, 2020, Accepted April 8, 2021*)

Abstract. Because of the limited land resources and preference of centralized services, more structures are often built close to each other, correspondingly yielding a demand that mitigates the dynamic responses of adjacent structures. Utilizing the intrinsic potential of the inerter to improve structural energy performances, an inerter-system chain is proposed for the adjacent single-degree-of-freedom structures, which forms a novel configuration featuring the reduction in input energy transmitted to the adjacent structures. The inerter-system chain is realized by two end-placed inerter-dashpot dampers and inter-placed spring-inerter-dashpot elements arranged in parallel. Stochastic energy balance analysis is conducted to derive a closed-form energy equation that reveals the energy basis of the inerter-system chain. An energy-based and bi-objective optimization strategy is developed with simultaneous consideration of displacement and energy performances, particularly easy-to-use design formulae being derived. The findings of this study show that a complete inerter-system chain exhibits a significant multi-reduction in the structural displacement, shear force, and dissipation energy burden. Particularly, the effectiveness of reducing the input power and vibrational energy transmitted into the entire structures counts on the series inerter-chain, which differentiates the proposed chain from alternative layouts. The proposed energy-based design framework is capable of minimizing the energy dissipation cost, with target displacement control demand satisfied.

Keywords: adjacent structure; energy balance; inerter; input power; optimal design

1. Introduction

Coupling the adjacent structures through the passive energy dissipation devices has been proven to be efficacious to mitigate the dynamic responses as well as reduce the chances of pounding (Miari *et al*. 2019). Dealing with the limited availability of the land resources and preferred centralized services, more building structures are built closely to each other, thereby yielding an increased demand that employs the interconnection to improve their dynamic resistant performances. A series of theoretical and experimental studies have been devoted to applicable energy dissipation forms and confirmed the effectiveness of the passive dampers for the response control of adjacent structures, including the viscous-damping (represented by a single dashpot (Bhaskararao and Jangid 2007, Farghaly 2015) or series arrangement of a spring and a dashpot (Xu *et al*. 1999), hysteretic (Ok *et al*. 2008), friction (Ng and Xu 2006), and viscoelastic (represented by a parallel arrangement of a spring and a dashpot) (Greco and Marano 2016) dampers. Optimization works (Ying *et al*. 2003, Ok *et al*. 2008, Cimellaro and Lopez-Garcia 2011) were presented in terms of the mechanical parameter design and the dampers' distribution pattern. Incorporating the new device called inerter with conventional dashpot and spring (Basili *et al*. 2018), a spring-dashpot-inerter system (SDIS) was proposed to pursuit the improved displacement control effect. The tuned inerter damper and tuned mass damper inerter were employed as multi-actuator systems for the vibration control of adjacent structures (Palacios-Quiñonero *et al*. 2019), clearly showing the superior performance and robustness in comparison with the tuned mass damper. Multiple tuned mass damper inerter system (De Domenico *et al*. 2020) linking two adjacent structures was presented as a seismic protection strategy for a significant acceleration control. Replacing the tuned mass by a liquid damper (Wang *et al*. 2020), a tuned liquid column damper inerter was developed to control the seismic response of adjacent high-rise buildings.

The mentioned inerter is essentially a two-terminal inertial element (Smith 2002) that provides a significant inertance with a mass unit to the controlled structure while introducing the negligible gravitational mass (Jiang *et al*. 2020, Zhao *et al*. 2020a). Ideally, the resistant force of this massless element is proportional to the relative acceleration between its two terminals and the inertance (Barredo *et al*. 2018, Huang *et al*. 2019). In retrospect, Kawamata (1973) introduced a liquid mass pump of which the inertance was obtained by a fluid-based inertial mechanism. In later years, Arakaki *et al*. (Arakaki *et al*. 1999a, b) proposed a ball-screw-based rotary damper aiming to amplify the effective viscous damping force. Generally, the representative realization approaches of the inerter include the ball-screw (Ikago *et al*. 2012), fluid (Kawamata 1973), rack-pinion

*Corresponding author, Ph.D.,
E-mail: zhaozhipeng@tongji.edu.cn

ISSN: 1738-1584 (Print), 1738-1991 (Online)

(Smith 2002), and electromagnetic (Asai *et al*. 2018) types, based on which some semi-active inerters (Chen *et al*. 2015) have been developed. In recent years, the inerter-based passive control configurations were proposed, among which the widely-analyzed are the tuned viscous mass damper (Ikago *et al*. 2012), tuned inerter damper (Lazar *et al*. 2016), tuned mass damper inerter (Marian and Giaralis 2014), and other lightweight-based tuned inerter systems (Marian and Giaralis 2017, Chen *et al*. 2019, Zhao *et al*. 2019b). Evaluating from the specific control performances, such as the displacement, acceleration, or the base shear force measurements, existing research (Takewaki *et al*. 2012, De Domenico *et al*. 2019a, Zhang *et al*. 2019, Zhao *et al*. 2019a) has clarified the advantageous features that the inerter systems achieve the lightweight control and the improved vibration mitigation effect. Applicable to the tuned viscous mass damper and tuned inerter damper, the dashpot-deformation amplification effect represents their basic benefit, with the dashpot deformation of the inerter systems being larger than the deformation of the entire inerter systems (Ikago *et al*. 2012, Zhang *et al*. 2020). The amplified dashpot deformation definitely improves the energy-dissipation efficiency for vibration control. Zhang *et al*. (2020) derived a closed-form equation to quantify the contribution of the inerter-system parameters to the amplification effect of the dashpot-deformation. From the perspective of the energy-based design, De Domenico *et al*. (De Domenico and Ricciardi 2018) designed an enhanced base isolation system including the tuned mass damper inerter by considering the energy-dissipation effect. Chen *et al*. (2018) incorporated the soil effect into the inerter-based structure and figured out the energy characteristics of the controlled structures. Sugiura *et al*. (2020) invented a novel inerter-based wave energy converter for the improved power generation performance over a wide range of wave frequencies. Inspired by the phenomenon of the energy benefit of inerters, Zhao *et al*. (2020b) derived a closed-form energy equation for a single-degree-of-freedom (SDOF) structure, and theoretically revealed the fact that an inerter inserted between the oscillating source and structural mass exhibits a reduction in the input energy to lighten the energy-dissipation burden of the entire controlled system and to reduce the control force of the employed control system. This considerable reduction in input energy of inerter-based structures differentiates the inerter-based control from the conventional dampers, which has great potential to the performance-improved control for more complex structures. Dealing with the control issue of the adjacent structures, the reduction of input energy transmitted into the controlled structures is a preferable solution. However, a reasonable configuration of the inerter system and its energy working basis are still unclear, which motivates the proposed control system in the following analysis.

In this study, a novel inerter-system chain (IS-chain) is proposed for the adjacent structures, which forms a configuration featuring an enhanced vibration control effect and a reduction of input energy transmitted to the adjacent structures. Stochastic energy balance analysis is performed to derive a closed-form energy equation that reveals the input-energy reduction principle of this inerter-system chain. Comparative studies were conducted to investigate the functionality of the inerter-system chain and its unique advantages over the existing control devices, including the viscous damper and single inerter system. Correspondingly, an energy-based optimization strategy is developed with simultaneous consideration of the displacement and energy responses. Finally, numerical examples are presented to validate the derived energy equation and proposed optimization strategy.

2. Simulation for adjacent structures with inerter-system chain

2.1 Single structure equipped with inerter

Subject to the base acceleration excitation a_g in the horizontal direction, a single structure equipped with an inerter with inertance m_{in} can be represented by an SDOF system, whose translation degree concentrates on the structural mass m. The oscillating vibration u of the structure is restricted by the structural damping c and stiffness k and the supplementary inerter. This mechanical system is relabeled in a non-dimensional form, including the circular frequency $\omega_0 = \sqrt{\frac{k}{m}}$, the inertance-mass ratio $\upsilon = \frac{m_{in}}{m}$, and inherent damping ratio $\zeta = \frac{c}{(2m\omega_0)}$.

The governing equation of motion for a single controlled structure (Fig. 1) is established according to the dynamic equilibrium condition

$$(1+\upsilon)\ddot{u} + 2\zeta\omega_0\dot{u} + \omega_0^2 u = -a_g \tag{1}$$

where u is the displacement of the equivalent mass of the SDOF structure relative to the ground. Laplace transformation (Crandall and Mark 2014) is used to rewrite the Eq. (1) in an algebraic form

$$s^2(1+\upsilon)U + 2s\zeta\omega_0 U + \omega_0^2 U = -A_g \tag{2}$$

where U and A_g are the Laplace transformation forms of u and a_g, respectively; The notation $s = i\omega$, where i is the imaginary unit and ω is the circular frequency of excitations. Solving the Eq. (2) with respect to U, the structural dynamic response can be finally obtained.

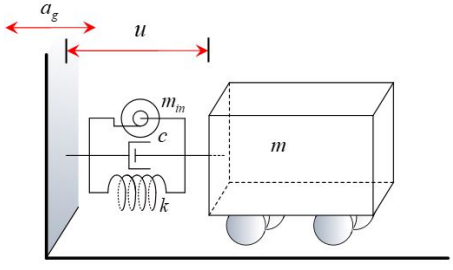

Fig. 1 Mechanical model of a single degree of freedom structure with an inerter

Corresponding transfer functions of the structural displacement H_U, velocity H_V, and shear force H_{SF} are determined by

$$H_U(i\omega) = \frac{U}{A_g}\bigg|_{s=i\omega} = -\frac{1}{s^2(1+\upsilon)+2s\zeta\omega_0+\omega_0^2}, \qquad H_V(i\omega) = s\cdot H_U(i\omega),$$
$$H_{SF}(i\omega) = \frac{\omega_0^2 U + 2s\zeta\omega_0 U}{A_g}\bigg|_{s=i\omega} = -\frac{\omega_0(2s\zeta+\omega_0)}{s^2(1+\upsilon)+2s\zeta\omega_0+\omega_0^2} \tag{3}$$

To provide an overall measurement for the dynamic performances covering the entire frequency domain, the mean-square quantities are derived for the displacement response σ_U^2, velocity response σ_{Vel}^2, and shear force response σ_{SF}^2 (Crandall and Mark 2014). The white noise with a constant power spectra density, S_0, is considered as the external excitation to simplify the stochastic response analysis, which further facilitates the derivation of analytical design formulae for the optimization of an inerter-system chain. The derived mean-square results are shown as

$$\sigma_U^2 = \int_{-\infty}^{\infty} |H_U(i\omega)|^2 S_0 d\omega,$$
$$\sigma_{Vel}^2 = \int_{-\infty}^{\infty} |H_{Vel}(i\omega)|^2 S_0 d\omega, \tag{4}$$
$$\sigma_{SF}^2 = \int_{-\infty}^{\infty} |H_{SF}(i\omega)|^2 S_0 d\omega$$

and simplified by the analytical integration in Eq. (4) (Crandall and Mark 2014)

$$\sigma_U^2 = \frac{\pi S_0}{2\zeta\omega_0^3}, \qquad \sigma_{Vel}^2 = \frac{\pi S_0}{2(1+\upsilon)\zeta\omega_0},$$
$$\sigma_{SF}^2 = \frac{\pi S_0(1+4\zeta^2+\upsilon)\omega_0}{2\zeta(1+\upsilon)} \tag{5}$$

In terms of the uncontrolled original structure without the inerter, the corresponding results, including the displacement, velocity, and shear force, can be easily obtained by substituting $\upsilon = 0$ into Eq. (5). Explained by the analytical solutions in Eq. (5) to the dynamic responses, the inerter directly connected to the ground or the mass exhibits no contribution to the displacement control, while observably depressing structural velocity (corresponding to the power of energy dissipation) and shear force.

on the primary structure u_p and the adjacent structure u_a. The primary structure (P-structure) is characterized by the concentrated mass m_p, structural stiffness k_p, and inherent damping coefficient $c_{p,0}$, whereas the adjacent structure (A-structure) is labeled by the concentrated mass m_a, structural stiffness k_a, and inherent damping coefficient $c_{a,0}$.

Born from the idea that employs a ground- or mass-connected inerter for vibration control, an inerter-system chain is introduced here, which basically consists of two nerter-dashpot dampers installed in the P-structure and A-structure, and an SDIS interconnected between the P- and A-structures (Fig. 2). The named inerter-dashpot damper refers to the parallel-spaced inerter with inertance $m_{in,i}$ and dashpot with damping coefficient c_i, where $i = p$ and a respectively represents the conditions for P- and A-structures. Note that the contribution of the structural inherent damping effect has been considered and involved in the damping effect of the added dashpot. The SDIS refers to a two-terminal inter-placed control system, the two terminals of which is used to link the inerter with inertance m_{in}, dashpot with damping coefficient c_d, and spring with stiffness k_d in parallel. The series arrangement of the inerter-dashpot and SDIS constitutes the so-called inerter-system chain, which is different from the widely analyzed SDIS and tuned mass damper inerter for adjacent structures. The proposed inerter-system chain can be realized by the ball-screw based inerter-dashpot damper (Ikago *et al*. 2012) that is connected with a spring in parallel. For construction, the inerter-system chain is suggested to be installed in the isolation layers of the adjacent isolated structures or on the first floor of the adjacent buildings. Table 1 describes the analyzed system (Fig. 2) in a non-dimensional form.

2.2.2 Governing equation and analytical solution

For the adjacent structures equipped with an inerter-system chain, the governing motions concentrate on the two degrees of freedom are given as

$$\begin{cases}(1+\upsilon)\ddot{u}_p + 2\varepsilon_p\omega_p\dot{u}_p + \omega_p^2 u_p - \mu(\ddot{u}_a - \ddot{u}_p) - 2\xi\omega_p(\dot{u}_a - \dot{u}_p) - \kappa\omega_p^2(u_a - u_p) = -a_g \\ (\beta+\nu)\ddot{u}_a + 2\beta\varepsilon_a\theta\omega_p\dot{u}_a + \beta\theta^2\omega_p^2 u_a + \mu(\ddot{u}_a - \ddot{u}_p) + 2\xi\omega_p(\dot{u}_a - \dot{u}_p) + \kappa\omega_p^2(u_a - u_p) = -\beta a_g\end{cases} \tag{6}$$

Inspecting this forced control system, the a_g-induced external force applied to controlled adjacent structures is the same for the uncontrolled ones, which is not increased by the additionally added inerter owing to its intrinsic mass amplification effect. By means of the Laplace transformation (Crandall and Mark 2014), the differential Eq. (6) can be converted into an algebraic form

$$\begin{cases}s^2(1+\upsilon)U_p + 2s\varepsilon_p\omega_p U_p + \omega_p^2 U_p - \mu s^2(U_a - U_p) - 2s\xi\omega_p(U_a - U_p) - \kappa\omega_p^2(U_a - U_p) = -A_g \\ s^2(\beta+\nu)U_a + 2s\beta\varepsilon_a\theta\omega_p U_a + \beta\theta^2\omega_p^2 U_a + s^2\mu(U_a - U_p) + 2s\xi\omega_p(U_a - U_p) + \kappa\omega_p^2(U_a - U_p) = -\beta A_g\end{cases} \tag{7}$$

2.2 Adjacent structures with inerter-system chain

2.2.1 Inerter-system chain and model of adjacent SDOF struzctures

Two SDOF structures are adopted to represent two adjacent structures, whose oscillating motions concentrate

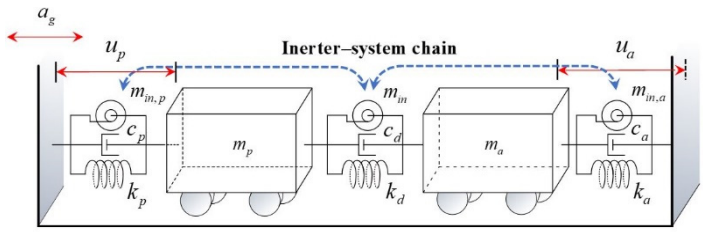

Fig. 2 Mechanical model of adjacent single degree of freedom structures with an inerter-system chain

Table 1 Parameters for adjacent structures controlled with inerter-system chain

Parameter		Definition	Description
Structures	P-structure	$\omega_p = \sqrt{\frac{k_p}{m_p}}$	P-structural circular frequency
		$\varepsilon_{p,0} = \frac{c_{p,0}}{2m_p\omega_p}$	Inherent damping ratio of P-structure
	A-structure	$\beta = \frac{m_a}{m_p}$	A-structural mass ratio
		$\theta = \frac{\sqrt{\frac{k_a}{m_a}}}{\omega_p}$	A-structural frequency ratio
		$\varepsilon_{a,0} = \frac{c_{a,0}}{2\beta m_p\theta\omega_p}$	Inherent damping ratio of A-structure
Inerter-system chain		$\mu = \frac{m_{in}}{m_p}$	Inertance mass ratio
		$\xi = \frac{c_d}{2m_p\omega_p}$	Nominal damping ratio
		$\kappa = \frac{k_d}{k_p}$	Stiffness ratio
		$\upsilon = \frac{m_{in,p}}{m_p}$	P-inertance mass ratio
		$\nu = \frac{m_{in,a}}{m_p}$	A-inertance mass ratio
		$\varepsilon_p = \frac{c_p}{2m_p\omega_p}$	Damping ratio of controlled P-structure
		$\varepsilon_a = \frac{c_a}{2\beta m_p\theta\omega_p}$	Damping ratio of controlled A-structure

where U_p and U_a is the Laplace transformation forms of u_p and u_a. As presented in Eq. (7), the concerned displacement responses with respect to U_p and U_a are solved as

$$\begin{cases} U_p(s) = \dfrac{-A_g\left(\left(\mu+\nu+\beta(1+\mu)\right)s^2 + 2\left(\xi+\beta(\xi+\theta\varepsilon_a)\right)\omega_p s + \left(\kappa+\beta(\theta^2+\kappa)\right)\omega_p^2\right)}{a_4s^4+a_3s^3+a_2s^2+a_1s+a_0} \\ U_a(s) = \dfrac{-A\left(\left(\mu+\beta(1+\mu+\upsilon)\right) + 2\left(\xi+\beta\xi+\beta\varepsilon_p\right)\omega_p s + (\beta+\kappa+\beta\kappa)\omega_p^2\right)}{a_4s^4+a_3s^3+a_2s^2+a_1s+a_0} \end{cases} \tag{8}$$

where the notations a_n $(n = 0, 1, 2, 3, 4)$ are given as

$$\begin{cases} a_4 = \nu(1+\upsilon)+\beta(1+\mu+\upsilon)+\mu(1+\nu+\upsilon) \\ a_3 = 2\left(\xi(1+\beta+\nu+\upsilon)+\beta\theta(1+\mu+\upsilon)\varepsilon_a+(\beta+\mu+\nu)\varepsilon_p\right)\omega_p \\ a_2 = \left(\mu+\nu+\kappa(1+\nu+\upsilon)+\beta\left(1+\kappa+\theta^2(1+\mu+\upsilon)\right)+4\xi\varepsilon_p+4\beta\theta\varepsilon_a\left(\xi+\varepsilon_p\right)\right)\omega_p^2 \\ a_1 = 2\left(\xi+\beta\theta^2\xi+\beta\theta(1+\kappa)\varepsilon_a+(\beta\theta^2+\kappa)\varepsilon_p\right)\omega_p^3 \\ a_0 = \left(\kappa+\beta\theta^2(1+\kappa)\right)\omega_p^4 \end{cases} \tag{9}$$

The relative deformation u_r focusing on the distance variation between the P- and A-structures is defined in the Laplace domain

$$U_r(s) = U_a(s) - U_p(s) \tag{10}$$

Adopting the same concept for the $H_U(i\omega)$ and $H_V(i\omega)$ in Eq. (3), the corresponding transfer functions for the controlled adjacent structures are determined in terms of the displacement, velocity, structural shear force H_{SF}, and control force of the SDIS H_{CF}

$$\begin{aligned}
&H_{U_p}(s)|s = i\omega = \frac{U_p(s)}{A_g(s)}, \qquad H_{U_a}(s)|s = i\omega = \frac{U_a(s)}{A_g(s)}, \qquad H_{U_r}(s)|s = i\omega = \frac{U_r(s)}{A_g(s)},\\
&H_{V_p}(s)|s = i\omega = \frac{sU_p(s)}{A_g(s)}, \qquad H_{V_a}(s)|s = i\omega = \frac{sU_a(s)}{A_g(s)}, \qquad H_{V_r}(s)|s = i\omega = \frac{sU_r(s)}{A_g(s)},\\
&H_{SF,p}(i\omega) = \left.\frac{\omega_p^2 U_p + 2s\varepsilon_p\omega_p U_p}{A_g}\right|_{s=i\omega}, \qquad H_{SF,a}(i\omega) = \left.\frac{\beta\theta^2\omega_p^2 U_a + 2s\beta\theta\varepsilon_a\omega_p U_a}{A_g}\right|_{s=i\omega},\\
&H_{CF}(i\omega) = \left.\frac{s^2\mu U_r + 2s\xi\omega_p U_r + \kappa\omega_p^2 U_r}{A_g}\right|_{s=i\omega}
\end{aligned} \tag{11}$$

where the scenarios for the P- and A-structures are distinguished by the subscript "p" and "a". The mean-square structural dynamic responses are derived by random vibration theory, including the $\sigma_{U_p}^2$, $\sigma_{U_a}^2$, $\sigma_{U_r}^2$, $\sigma_{V_p}^2$, $\sigma_{V_a}^2$, $\sigma_{V_r}^2$, $\sigma_{SF,p}^2$, $\sigma_{SF.a}^2$, and σ_{CF}^2. Employing the integration process, the velocity responses (i.e., $\sigma_{V_p}^2$, $\sigma_{V_r}^2$, and $\sigma_{V_a}^2$) are the derivation of energy equations in the next section (Crandall derived in closed form for and Mark 2014)

$$\begin{aligned}
&E_{k,s}(t) + E_{e,s}(t) + E_{k,inerter}(t) + E_{e,SDIS}(t)\\
&+E_{d,SDIS}(t) + E_{d,P}(t) + E_{d,A}(t) = E_{input}(t)
\end{aligned} \tag{13}$$

where

$$E_{k,s}(t) = \int_0^t \left(\dot{u}_p\ddot{u}_p + \dot{u}_a\ddot{u}_a\right)d\tau\,,$$

$$E_{e,s}(t) = \int_0^t \left(\dot{u}_p\omega_p^2 u_p + \dot{u}_a\theta^2\omega_p^2 u_a\right)d\tau\,,$$

$$\text{and} \quad E_{input}(t) = \int_0^t \left(\dot{u}_p + \beta\dot{u}_a\right)a_g d\tau$$

are the structural kinetic energy, elastic strain energy, and input energy, respectively

$$E_{k,inerter}(t) = \int_0^t \left(\dot{u}_p v\ddot{u}_p + \dot{u}_a v\ddot{u}_a + \dot{u}_r\mu\ddot{u}_r\right)d\tau$$

$$\text{and} \quad E_{e,SDIS}(t) = \int_0^t u_r\cdot\kappa\omega_p^2\dot{u}_r d\tau$$

$$\begin{cases}
\sigma_{V_p}^2 = \dfrac{\pi S_0\left(\begin{array}{l}\left(\kappa+\beta(\theta^2+\kappa)\right)^2(a_2a_3-a_1a_4)\omega_p^4 +\\ a_0\left((\beta+\mu+\beta\mu+\nu)^2a_1 - 2a_3\left(\begin{array}{l}\kappa\mu+\kappa\nu-2\xi^2+\beta(\theta^2(\mu+\nu)+\kappa(1+2\mu+\nu)-4\xi^2)+\\ \beta^2(\kappa+\kappa\mu+\theta^2(1+\mu)-2\xi^2)-4\beta(1+\beta)\theta\xi\varepsilon_a-2\beta^2\theta^2\varepsilon_a^2\end{array}\right)\omega_p^2\right)\end{array}\right)}{a_0(a_1a_2a_3-a_0a_3^2-a_1^2a_4)}\\
\sigma_{V_a}^2 = \dfrac{\pi S_0\left(\begin{array}{l}(\beta+\kappa+\beta\kappa)^2(a_2a_3-a_1a_4)\omega_p^4 +\\ a_0\left(\left(\mu+\beta(1+\mu+\upsilon)\right)^2a_1 - 2a_3\left(\begin{array}{l}\kappa\mu-2\xi^2+\beta^2\left(1+\mu-2\xi^2+\upsilon+\kappa(1+\mu+\upsilon)\right)+\\ \beta\left(\mu-4\xi^2+\kappa(1+2\mu+\upsilon)\right)-4\beta(1+\beta)\xi\varepsilon_p-2\beta^2\varepsilon_p^2\end{array}\right)\omega_p^2\right)\end{array}\right)}{a_0(a_1a_2a_3-a_0a_3^2-a_1^2a_4)}\\
\sigma_{V_r}^2 = \dfrac{\pi S_0\left(\begin{array}{l}\beta^2(-1+\theta^2)^2(a_2a_3-a_1a_4)\omega_p^4 +\\ a_0\left((\nu-\beta\upsilon)^2a_1 + 2\beta a_3\left(-(-1+\theta^2)(\nu-\beta\upsilon)+2\beta\theta^2\varepsilon_a^2-4\beta\theta\varepsilon_a\varepsilon_p+2\beta\varepsilon_p^2\right)\omega_p^2\right)\end{array}\right)}{a_0(a_1a_2a_3-a_0a_3^2-a_1^2a_4)}
\end{cases} \tag{12}$$

3. Reduction in input energy and optimal design framework

3.1 Closed-form energy equation

The energy-based analysis yields an overall measurement of the structural performance and energy cost for the vibration control (De Domenico and Ricciardi 2019, Javidialesaadi and Wierschem 2019). To characterize the energy-related features of the controlled adjacent structures, an energy analysis model is established by pre-multiplying Eq. (6) by $\{\dot{u}_p, \dot{u}_a\}^T$, and then integrating over the time domain. The a_g-induced energy input into the entire adjacent structures is evaluated as the sum of distributions are the kinetic energy of the inerters distributed on the inerter chain and the elastic strain energy of the SDIS, respectively; and $E_{d,SDIS}(t) = \int_0^t \dot{u}_r\cdot 2\xi\omega_p\dot{u}_r d\tau$, $E_{d,P}(t) = \int_0^t \dot{u}_p\cdot 2\varepsilon_p\omega_p\dot{u}_p d\tau$, and $E_{d,A}(t) = \int_0^t \dot{u}_a\cdot 2\beta\theta\varepsilon_a\omega_p\dot{u}_a d\tau$ are the viscous damping energies dissipated by dashpots in the SDIS, P-structure, and A-structure. t denotes the duration of the integral, whereas τ is the integration variable. For a unit time, the integrated function e_x represents the rate of energy E_x (i.e., the power) at the time instance τ, where the subscript "x" is a generic symbol representing the different types of energies in Eq. (13) (Uang and Bertero 1988, Reggio and Angelis 2015). Correspondingly, the energy balance per unit time or the

power balance can be established as (De Domenico *et al*. 2019b)

$$e_{k,s} + e_{e,s} + e_{k,inerter} + e_{e,SDIS} + e_{d,SDIS} + e_{d,P} + e_{d,A} = e_{input} \tag{14}$$

Supposing a stochastic excitation a_g in assumption of ergodicity, the expectation operator $E[\cdot]$ is employed in the integrated e_x in Eq. (14). The input power and dissipation power are evaluated, of which the expected values in the stationary condition are summarized as (Reggio and Angelis 2015)

$$\begin{aligned} E\left[e_{d,P}\right] &= 2\varepsilon_p\omega_p E\left[\dot{u}_p\dot{u}_p\right] = 2\varepsilon_p\omega_p\sigma_{V_p}^2, \\ \mathrm{E}\left[e_{d,A}\right] &= 2\beta\theta\varepsilon_a\omega_p E[\dot{u}_a\dot{u}_a] = 2\beta\theta\varepsilon_a\omega_p\sigma_{V_a}^2, \\ E\left[e_{d,SDIS}\right] &= 2\xi\omega_p E[\dot{u}_r\dot{u}_r] = 2\xi\omega_p\sigma_{V_r}^2 \end{aligned} \tag{15}$$

and

$$E\left[e_{k,s}\right] = E\left[e_{e,s}\right] = E\left[e_{k,inerter}\right] = E\left[e_{e,SDIS}\right] = 0 \tag{16}$$

consistently with the conservation of mechanical energy. The non-zero items $E\left[e_{d,P}\right]$, $E\left[e_{d,A}\right]$, and $E\left[e_{d,SDIS}\right]$ denote energy dissipation powers of the P-structure, the A-structure, and the SDIS, sum of which composes the input power of the entire controlled adjacent structures in the stationary condition

$$\begin{aligned} E\left[e_{input}\right] &= E\left[e_{d,P}\right] + \mathrm{E}\left[e_{d,A}\right] + E\left[e_{d,SDIS}\right] \\ &= 2\xi\omega_p\sigma_{V_r}^2 + 2\varepsilon_p\omega_p\sigma_{V_p}^2 + 2\beta\theta\varepsilon_a\omega_p\sigma_{V_a}^2 \end{aligned} \tag{17}$$

Substituting the closed-form expressions $\sigma_{V_p}^2$, $\sigma_{V_a}^2$, and $\sigma_{V_r}^2$ of Eq. (12) into Eq. (17), the power balance in the stationary condition is finally reported in a concise manner. In this process, the derivation of the formula involves algebraic operations on symbolic variables, from which it is not difficult to obtain the final expression

$$E\left[e_{input}\right] = 2\xi\omega_p\sigma_{V_r}^2 + 2\varepsilon_p\omega_p\sigma_{V_p}^2 + 2\beta\theta\varepsilon_a\omega_p\sigma_{V_a}^2 = (\pi S_0)\cdot\frac{\beta+\mu+2\beta\mu+\nu+\beta^2(1+\mu+\upsilon)}{\nu(1+\upsilon)+\beta(1+\mu+\upsilon)+\mu(1+\nu+\upsilon)} \tag{18}$$

With regard to an uncontrolled P-structure, the original input power can be directly obtained as a special case of Eq. (18) by designating $\beta = \mu = \nu = \upsilon = 0$, which can be expressed as

$$E\left[e_{input,0}\right] = 2\varepsilon_{p,0}\omega_p\sigma_{V_p,0}^2 = \pi S_0 \tag{19}$$

where the subscript '0' refers to the uncontrolled one treated as a reference in this study.

For a viscous damping element, its velocity response is closely related to the dissipation power and the quantity of dissipated energy. In this regard, the dimensional velocity response ratios of the P-structure α_p, A-structure α_a, and the interspace α_r are defined, whereas the normalized *Input Energy Index* η is given as

$$\alpha_p = \frac{\sigma_{V_p}}{\sigma_{V_p,0}}, \qquad \alpha_a = \frac{\sigma_{V_a}}{\sigma_{V_a,0}}, \qquad \alpha_r = \frac{\sigma_{V_r}}{\sigma_{V_p,0}}, \qquad \eta = \frac{E\left[e_{input}\right]}{E\left[e_{input,0}\right]} \tag{20}$$

where $\sigma_{V_p,0} = \sqrt{\frac{\pi S_0}{2\varepsilon_p\omega_p}}$, $\sigma_{V_a,0} = \sqrt{\frac{\pi S_0}{2\beta\theta\varepsilon_a\omega_p}}$. Note that the α_r is defined by deriving the root mean square of the velocity response of P-structure for the normalization. Dividing both sides of Eq. (18) by πS_0, the left-hand side is derived as

$$\begin{aligned} &\frac{2\xi\omega_p\sigma_{V_r}^2 + 2\varepsilon_p\omega_p\sigma_{V_p}^2 + 2\beta\theta\varepsilon_a\omega_p\sigma_{V_a}^2}{\pi S_0} \\ &= \frac{\xi}{\varepsilon_p}\frac{\sigma_{V_r}^2}{\frac{\pi S_0}{2\varepsilon_p\omega_p}} + \frac{\sigma_{V_p}^2}{\frac{\pi S_0}{2\varepsilon_p\omega_p}} + \frac{\sigma_{V_a}^2}{\frac{\pi S_0}{2\beta\theta\varepsilon_a\omega_p}} = \alpha_r^2\frac{\xi}{\varepsilon_p} + \alpha_p^2 + \alpha_a^2 \end{aligned} \tag{21}$$

and the right-hand side is

$$\begin{aligned} \eta &= \frac{E\left[e_{input}\right]}{\pi S_0} = \frac{E\left[e_{input}\right]}{E\left[e_{input,0}\right]} \\ &= \frac{\beta+\mu+2\beta\mu+\nu+\beta^2(1+\mu+\upsilon)}{\nu(1+\upsilon)+\beta(1+\mu+\upsilon)+\mu(1+\nu+\upsilon)} \end{aligned} \tag{22}$$

Referring to the final results in Eqs. (21) and (22), the energy equation is finally read as

$$\alpha_r^2\frac{\xi}{\varepsilon_p} + \alpha_p^2 + \alpha_a^2 = \eta \tag{23}$$

This energy equation is established on the basis of the stochastic power balance of controlled adjacent structures for a time instance, theoretically clarifying the quantitative relationship between input power, dissipation powers of various mechanical components, and parameters of inerter-system chain. For the controlled or uncontrolled adjacent structures subject to the same excitation (guaranteeing the same duration), the explained theoretical basis of the power is applicable for the understanding of the energy relationship.

Inspecting the input energy index η in Eq. (22), the input power, reflecting the total burden or the requirement of energy dissipation, is basically determined by the entire gravitational masses including those of P-structure and A-structure, more importantly, is also positively related to the employed inertances distributed among the inerter chain. In this sense, the contribution of inerters for the input power reduction differentiates the inerter chain-based adjacent structures and conventional ones that only counts on the gravitational masses.

Dealing with the potential of the inter-spaced inerter μ, the partial derivative of η with respect to the μ is given

$$\frac{\partial\eta}{\partial\mu} = -\frac{(\nu-\beta\upsilon)^2}{(\beta+\mu+\beta\mu+\nu+\mu\nu+(\beta+\mu+\nu)\upsilon)^2} \leq 0 \tag{24}$$

Table 2 Results of input energy index η for adjacent structures with inerter-system chain in special cases

Special cases		Input energy index η
Uncontrolled adjacent structures	$\mu = \nu = \upsilon = 0$	$1+\beta$
Controlled by inerter-system chain	Incomplete chain $\mu = 0$	$\frac{\beta^2}{\beta+\nu}+\frac{1}{1+\upsilon}$
	Incomplete chain $\upsilon = \nu = 0$	$1+\beta$
	Complete chain $\mu = \infty$	$\frac{(1+\beta)^2}{1+\beta+\nu+\upsilon} < 1+\beta$

which implies the fact that a larger inertance employed between the two adjacent structure is beneficial to reduce the input power and corresponding burden of the energy dissipation. Table 2 summarizes the results of η in some listed special cases, which can be unified in Eq. (23). It is addressed that a complete inerter-system chain that directly links the adjacent structure and oscillating source (ground) is indispensable to reduce the input power and energy burden. The detailed functionality of these inertances will be discussed in the next section.

3.2 Dynamic performances of inerter-system chain

The installation of the proposed inerter-system chain facilitates the adjustment of the energy (or power) performance of the adjacent structures, which has been clearly stated by the Eq. (23) for the first time. Counting on the synthetic mechanism within the inerter-system chain, especially the series-linked inerters, the oscillating adjacent structures can be suppressed in an efficient manner. For investigating the contribution of the inerter-system chain for vibration control, comprehensive parametric analysis in terms of the displacement, energy, and structural shear force is conducted here, which also aims to seek a rational design strategy.

The energy performance is evaluated by the defined measurements, including the α_p^2 for P-structure, α_a^2 for A-structure, and $\alpha_r^2\frac{\xi}{\varepsilon_p}$ for the inter space. For the displacement performance, structural displacement ratios, γ_p, γ_a, and γ_r are considered together, respectively denoting the condition of P-structure, A-structure, and the interspace

$$\gamma_p = \frac{\sigma_{U_p}}{\sigma_{U_p,0}}, \qquad \gamma_a = \frac{\sigma_{U_a}}{\sigma_{U_a,0}}, \qquad \gamma_r = \frac{\sigma_{U_r}}{\sigma_{U_r,0}} \tag{25}$$

The structural shear force ratios are given for the adjacent structures, $\lambda_{SF,_p}$ and $\lambda_{SF,a}$, whereas the control force ratio λ_{CF}, namely evaluating the control cost, is defined for the SDIS

$$\lambda_{SF,p} = \frac{\sigma_{SF,p}}{\sigma_{SF,p0}}, \qquad \lambda_{SF,a} = \frac{\sigma_{SF,a}}{\sigma_{SF,a0}}, \qquad \lambda_{CF} = \frac{\sigma_{CF}}{\sigma_{SF,p0}} \tag{26}$$

Unless otherwise stated in this research work, the subscript "0" represents the corresponding condition of the uncontrolled structure. The λ_{CF} is normalized by dividing the structural shear force of an uncontrolled P-structure. These representative indices associated with the dynamic performance of inerter-based adjacent structures are summarized in Table 3.

3.2.1 Contribution of inter-placed inerter

Taking $\theta = 0.70$ for instance of a flexible adjacent structure, three representative adjacent structures are considered, including $\beta = 0.75$ (Case I), $\beta = 1.00$ (Case II), and $\beta = 1.25$ (Case III). The inherent damping ratio of the original uncontrolled structures is assumed as $\varepsilon_{p,0} = \varepsilon_{a,0} = 0.02$. The contribution of the inerter in SDIS for vibration control is evaluated systematically from the perspective of the mentioned energy, displacement, structural shear force, and control force (see Table 3). The variations of concerned indices are calculated with continuously changed μ (inerter) by means of the solutions in Section 2.2.2. Fig. 3 shows the corresponding results in a line-plot for inerter-system chain with $\varepsilon_p = \varepsilon_a = 0.05$ and $\upsilon = \nu = 0.25$ for instance. The analyzed variation trend and principle are applicable for the other parameter sets. In this precondition, the inter-placed linking spring and dashpot, respectively denoted by κ and ξ, are optimized by minimizing the dissipation power (or the burden) of the P-structure for providing an optimal performance to the primary structure for instance. With the aid of a larger inertance μ employed in the SDIS, the flexible A-structure exhibits lower dynamic responses in terms of the dissipation burden (Fig. 3(a)), displacement (Fig. 3(b)), and shear force

Table 3 Evaluation indices for adjacent structures with inerter-system chain8

Index		Description
Displacement	γ_p, γ_a	Displacement response ratio of P- and A-structures
	γ_r	Relative displacement ratio of inter space
Force	$\lambda_{SF,p}$, $\lambda_{SF,a}$	Structural shear force ratio of P- and A-structures
	λ_{CF}	Control force ratio of SDIS
Energy	α_p^2, α_a^2	Dissipation power ratios of P- and A-structures
	$\frac{\alpha_r^2\xi}{\varepsilon_p}$	Dissipation power ratio of SDIS
	η	Input energy (or power) index

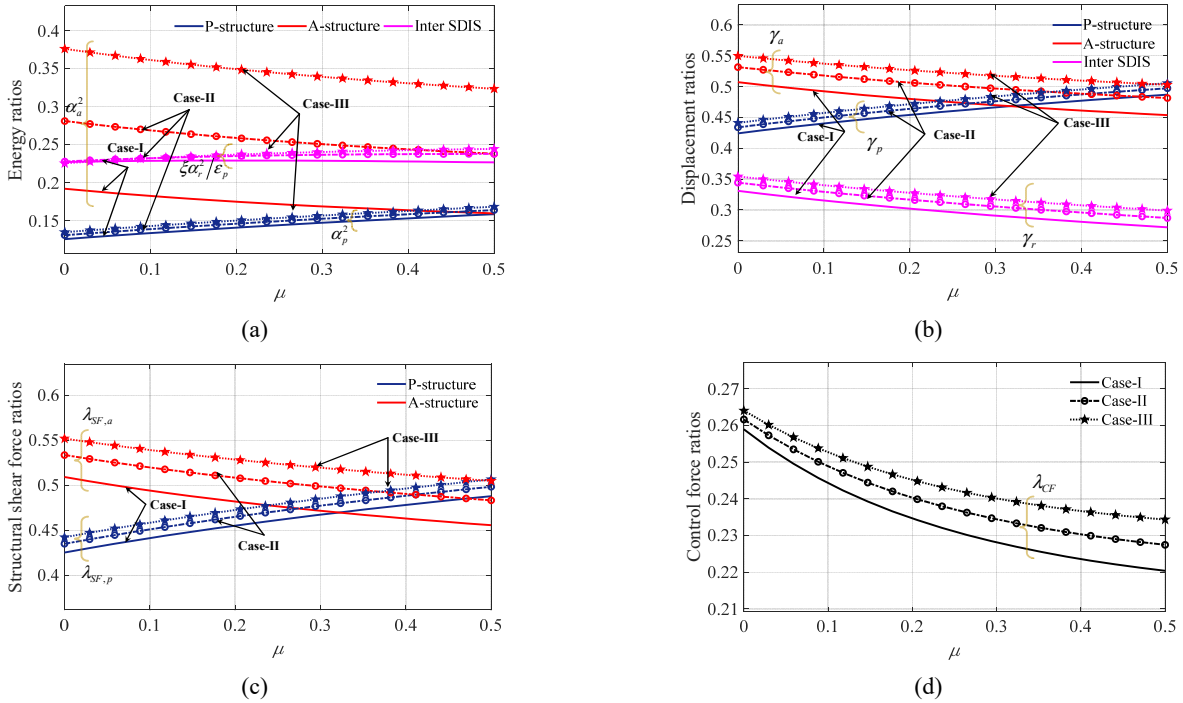

Fig. 3 Lines plots of dynamic performances for the adjacent structures in Case-I to III controlled by the inerter-system chain for $\varepsilon_p = \varepsilon_a = 0.05$, $\upsilon = \nu = 0.25$, κ and ξ for optimized α_p^2, and $\mu \in [0,0.5]$. (a) Structural power ratios $\alpha_r^2 \frac{\xi}{\varepsilon_p}$, α_p^2, and α_a^2; (b) displacement ratios γ_r, γ_p, and γ_a; (c) structural shear force ratio $\theta_{SF,p}$ and $\theta_{SF,a}$; (d) structural control force ratio θ_{CF}

(Fig. 3(c)). At the same time, the relative oscillating vibration between the adjacent structure is suppressed effectively, which results from the improved dissipation power of the SDIS and a stronger interconnection SDIS enhanced by the increased μ. Owing to this increased μ, more energy is filtered into the P-structure, which causes a slight increase of the displacement and shear force responses. Dealing with this accompanying and negative influence, a performance-demand-based design is suggested to determine the employed inerter of SDIS providing target performances for adjacent structures. Apart from the contribution to the control performance, it is consistent with the derived energy equation that the energy dissipation burden is reduced by the increased μ, correspondingly saving the control cost evaluated by the control force in Fig. 3(d).

3.2.2 Contribution of end-placed inerters

To scrutinize the correlation control effect of the end-placed inerters, i.e., the υ for the P-structure, and ν for the A-structure, the variations of systematical dynamic performances against variable υ and ν are calculated and visualized in surf- and bar-forms in Fig. 4. The adjacent structure in Case I is considered for illustration, where the inertance-mass ratio $\mu = 0.25$ and corresponding κ and ξ are selected from the optimization results in Fig. 3, for the trade-off control of both the P- and A-structures. For the energy performance in Fig. 4(a), the collaboration of the two end-placed inerters notably lightens the entire input power η (related to total input energy) from 1.75 to 0.82. Especially, the energy dissipation burden imposed on the adjacent structures is reduced continuously. In terms of the SDIS, its functionality for energy dissipation and vibration control is enhanced in Fig. 4(b), where the percentage dissipation power contributed by the SDIS is nearly doubled (from 0.21 to 0.39). Benefitting from the advantage that less energy is input and required for dissipation, the displacement and structural shear force responses are suppressed by the end-placed inerters. Especially indicated by the yellow and black arrows in the Fig. 4(c) and (d), the inerter ν for the flexible A-structure is dominant to remarkably reduce the displacement and shear force responses. The implementation of this inerter can be viewed as the increase of the tuned mass without any gradational quantity, correspondingly resulting in this reduction. Concomitantly, the increase of ν is accompanied by a larger relative oscillation between the adjacent structures, while the increased γ_r is still lower than the controlled adjacent structures without the aid of ν and υ.

3.2.3 Contribution of stiffness and damping effects in SDIS

Given that the series linked inerter is beneficial for multi-objective control of the adjacent structures, it is useful for completeness to investigate the variation pattern of the concerned dynamic performances against the variable stiffness ratio κ and nominal damping ratio ξ. The Case I is considered for the inerter-chain with medium inertances ($\mu = \upsilon = \nu = 0.25$) selected from the parametric analysis above, of which the results are plotted in a surf form in

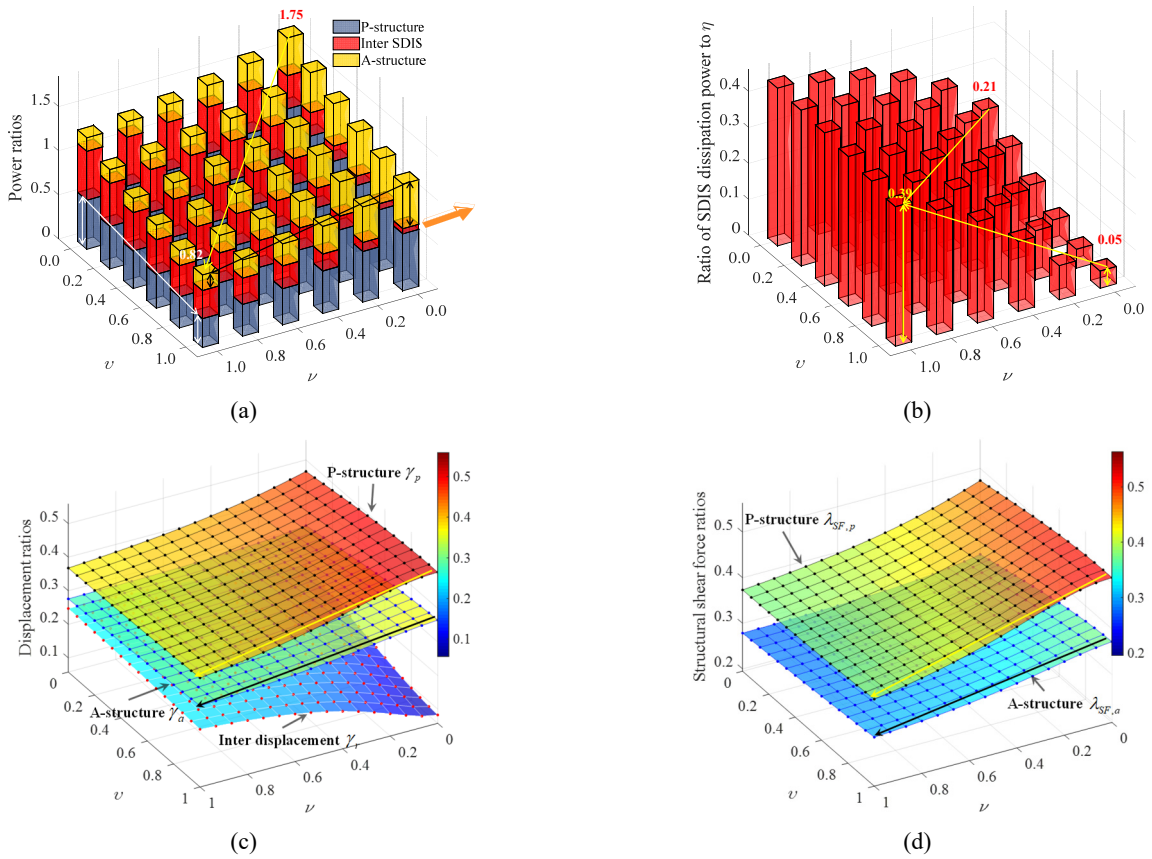

Fig. 4 Plots of dynamic performances for the adjacent structures in Case I controlled by the inerter-system chain for $\varepsilon_p = \varepsilon_a = 0.1$, $\kappa = 0.1$, $\xi = 0.1$, $\mu = 0.25$, $\upsilon \in [0, 1.0]$, and $\nu \in [0, 1.0]$. (a) Structural power ratios $\alpha_r^2 \frac{\xi}{\varepsilon_p}$, α_p^2, and α_a^2; (b) ratio of dissipation power of SDIS $\alpha_r^2 \frac{\xi}{\varepsilon_p}$ to the input energy index η; (c) displacement ratios γ_r, γ_p, and γ_a; (d) structural shear force ratio $\theta_{SF,p}$ and $\theta_{SF,a}$

Fig. 5. By inspection of the energy (Fig. 5(a)), displacement (Fig. 5(b)), and structural shear force (Fig. 5(c)) performances, it is noted that the locations of the minimum γ_p (marked by a white triangle), α_p^2, and $\lambda_{SF,p}$ almost coincide with each other, at the same time referring to the areas denoting low dynamic responses of the A-structure. Concomitantly, the SDIS exhibits a high efficiency of energy dissipation, a limited relative deformation, and a low-level control force ($\lambda_{CF} \approx 0.25$ in Fig. 5(d)). To investigate the applicability of obtained results under the assumption of white-noise for the case of seismic excitations, a filtered white noise using the Kanai-Tajimi filter for the firm soil condition (Kiureghian and Neuenhofer 1992) is adopted for comparison. Considering the two types of excitations, the energy-based performances of the P- and A-structures are shown in Fig. 6. By investigating the results of the α_p^2 and α_a^2, it can be found that the dynamic performances of inerter-based adjacent structures subject to the filtered white noise are close to those of the white-noise case. Given the same variation patterns of the α_p^2 or α_a^2 against the κ and ξ in the cases of two excitations, the assumption of white noise can bring about a satisfactory optimal design of an inerter-system chain for building structures subject to seismic excitations. The parametric analysis results, especially the preselected optimal condition of the inerter-system chain, can facilitate the optimal design in the next section.

3.3 Design formulations

Following a phenomenon-inspired design philosophy, the optimal design of the proposed inerter-system chain requires the meet of the control requirement with a tradeoff between the structural performance and the control burden of the energy dissipation, potentially reducing or even avoiding structural damage due to the excessive energy accumulation. Before the optimization, the undetermined key parameters should be clarified for the inerter-system chain, which includes the υ and ε_p for the P-end of the chain, the ν and ε_a for the A-end of the chain, and μ, ξ, and κ for the SDIS. As revealed in the derived energy Eq. (23), the input and dissipation powers are dependent on the parameters of the inerter-system chain, especially the inertance ratios. In this situation, it is a priority that the input power of the entire adjacent structures or the dissipation power contributed by the P- or A-structures should be minimized in the premise of representative control target. Considering the similar variation pattern of the displacement and structural shear force responses, the displacement performance, i.e., the γ_p, γ_r, and γ_a are

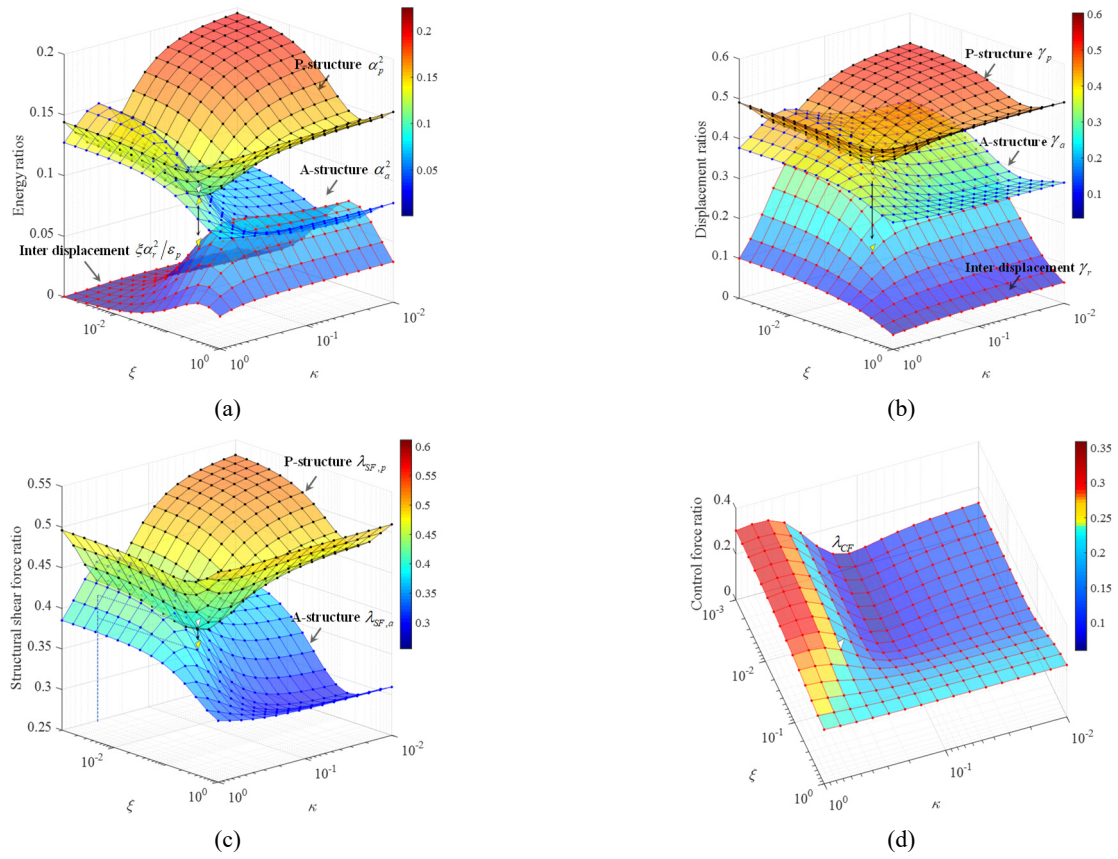

Fig. 5 Surf plots of dynamic performances for the adjacent structures in Case I controlled by the inerter-system chain for $\varepsilon_p = \varepsilon_a = 0.1$, $\mu = \upsilon = \nu = 0.25$, $\kappa \in [0.01, 1.0]$, and $\xi \in [0.001, 1.0]$. (a) Structural power ratios $\alpha_r^2 \frac{\xi}{\varepsilon_p}$, α_p^2, and α_a^2; (b) displacement ratios γ_r, γ_p, and γ_a; (c) structural shear force ratio $\theta_{SF,p}$ and $\theta_{SF,a}$; (d) structural control force ratio θ_{CF}

selected as for a systematical evaluation. In summary, a nonlinear constrained single-objective optimization problem is established for multiple variables

$$\begin{cases} \underset{\eta,\alpha_p^2,\alpha_a^2,or\frac{\xi\alpha_r^2}{\varepsilon_p}}{\text{minimize}}\ Energy\ control\ cost \\ \text{subject to} \begin{cases} \gamma_p \le \gamma_{p,t} \\ \gamma_r \le \gamma_{r,t} \\ \gamma_a \le \gamma_{a,t} \end{cases} \end{cases} \tag{27}$$

where the subscript "t" denotes the target demand of the displacement. The energy performance, related to the P-, A-structures, and their interspace are all optional selections for the optimization, whereas the P-structure is suggested according to the results from the parametric analysis. In this design condition, the minimization of the α_p^2 is theoretically equivalent to the equilibrium condition (see Fig. 5) that the partial derivatives of α_p^2 with respect to the ξ and κ are set zero. Eq. (27) is rewritten in the mathematical form as

$$\begin{cases} \text{minimize Energy control cost} \to \alpha_p^2 \\ \text{subject to} \begin{cases} \gamma_p \le \gamma_{p,t} \\ \gamma_r \le \gamma_{r,t} \\ \gamma_a \le \gamma_{a,t} \end{cases} \end{cases} \to \begin{cases} \frac{\partial \alpha_p^2}{\partial \xi} = 0, \frac{\partial \alpha_p^2}{\partial \kappa} = 0 \\ \text{subject to} \begin{cases} \gamma_p \le \gamma_{p,t} \\ \gamma_r \le \gamma_{r,t} \\ \gamma_a \le \gamma_{a,t} \end{cases} \end{cases} \tag{28}$$

to which the solution has been highlighted by the white triangle in Fig. 5. This optimization problem can be also solved in a numerical form by using the standard pattern search algorithm "fmincon" in MATLAB® to determine optimal parameters. The Kanai-Tajimi model (Kiureghian and Neuenhofer 1992) can be employed as excitations for this numerical optimization to simulate the seismic ground motions.

Apart from the numerical solution above, an analytical design formulation is given for the conceptual design and understanding. Substituting the closed-form expression of $\sigma_{\dot{V}_p}^2$ (related to α_p^2) of the Eq. (12) into the Eq. (27), the values of ξ and κ can be determined theoretically, although the detailed expression is complicated. Considering a simplified condition where the damping ratios added to the P- and A-structures are assumed zero $\varepsilon_p = \varepsilon_a = 0$, the ξ and κ can be preliminary designed as

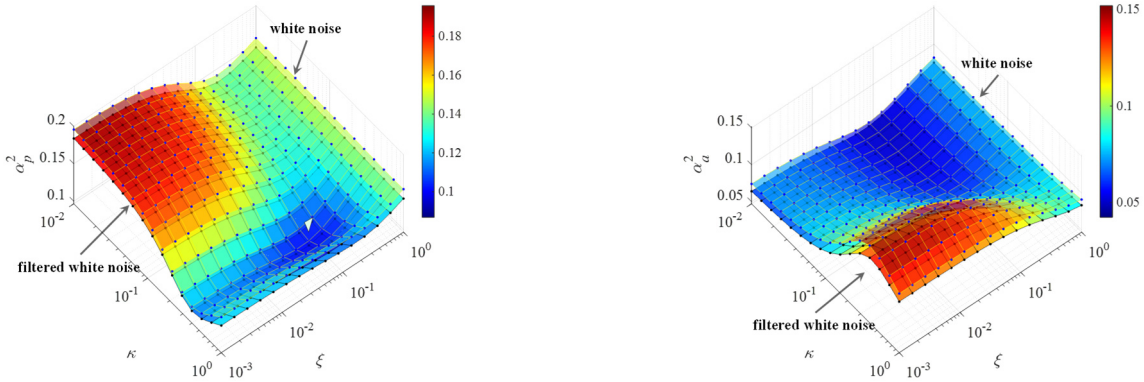

(a) (b)

Fig. 6 Surf plots of energy-based performances for the adjacent structures in Case I controlled by the inerter-system chain for $\varepsilon_p = \varepsilon_a = 0.1$, $\mu = \upsilon = \nu = 0.25$, $\kappa \in [0.01, 1.0]$, and $\xi \in [0.001, 1.0]$ under the white noise and filtered white noise. (a) α_p^2 and (b) α_a^2

$$\begin{cases} \kappa = \dfrac{\mu + \beta^2\theta^2\mu + \nu + \beta\left(1 - \theta^2 + \mu + \theta^2(\mu - \upsilon)\right)}{(1+\beta)(1+\beta+\nu+\upsilon)} \\ \xi = \dfrac{(\beta + \mu + \beta\mu + \nu)\left(\nu + \beta(1 - \theta^2 - \theta^2\upsilon)\right)}{2\sqrt{(1+\beta)^2(1+\beta\theta^2)(1+\beta+\nu+\upsilon)\left(\nu(1+\upsilon) + \beta(1+\mu+\upsilon) + \mu(1+\nu+\upsilon)\right)}} \end{cases} \tag{29}$$

which can be further used as the optimized relationship between the ξ, κ, and μ. Given the benefit of end-placed inerters for the reduction in the input power and shear force as shown in Eqs. (5) and (18), two end-placed inerters with large inertances are accompanied by a significant reduction effect. As revealed in the closed-form energy Eqs. (5) and (23), the increase of inertance implemented for the grounded inerter is accompanied by a significant reduction of input energy. The related inertance-mass ratios, υ and ν, are optimized to the upper boundary of their feasible domain. In practice, the value of this upper boundary can be determined on the basis of the feasibility of processing an inerter device with such a large inertance. The inertance-mass ratio μ of the SDIS can be optimized by solving the design Eq. (27) to meet the constraint condition of the target control demand.

4. Design examples

Employing the energy-based optimal design principle, typical adjacent structures are controlled by the designed inerter-system chain to pursuit dual benefits of the displacement and energy performances. Comparative studies between the inerter-system chain and the dashpot-spring system are performed to distinguish the functionality of inerter-chain. Consider the analyzed Case I with $\theta = 0.70$ and $\beta = 0.75$, the displacement constraint target is determined as 0.75 in Case A and 0.65 in Case B, where the end-placed inerters ν and υ are, respectively, optimized to their upper boundaries (Zhao *et al*. 2020b) as 0.25 and 0.50. The primary structure is described with structural mass $m_p = 20$ ton (Zhang *et al*. 2020) and oscillating period 1.0 s. Dealing with the targeted investigation of the inerters among the inerter-system chain, the damping ratio f the controlled P- and A-structures are assumed $\varepsilon_p = \varepsilon_a = 0.05$ as same as the inherent damping ratio of uncontrolled ones. In light of the determined values of γ_t in each case, the undetermined SDIS in the inerter-system chain is designed by minimizing the entire input energy η and obtained by solving the design problem in Eq. (27). As summarized in Table 4, the combination of a series of large inertances υ, ν, and optimized μ are beneficial to reduce the energy transmitted to the entire adjacent structures (corresponding to low η). Note that the ξ and κ designed by Eq. (29) match the numerical results, implying that analytical design formulations derived for zero-damped adjacent structures potentially reveal the optimized relationship between the undetermined μ, ξ, and κ. And the design criterion of minimization of η yields a rational approach to design the

Table 4 Designed inerter-system chain parameters and structural response results

Case IDS	Pre-specified		Series inerters		SDIS			η
	$\gamma_{p,t}$	$\gamma_{a,t}$	υ	ν	μ	ξ	κ	
Case A	0.75	0.75	0.25	0.25	0.381	0.095 (0.104)*	0.373 (0.374)	1.365
Case B	0.65	0.65	0.50	0.50	0.148	0.087 (0.097)	0.201 (0.207)	1.119

*The values in the small brackets are calculated from Eq. (29)

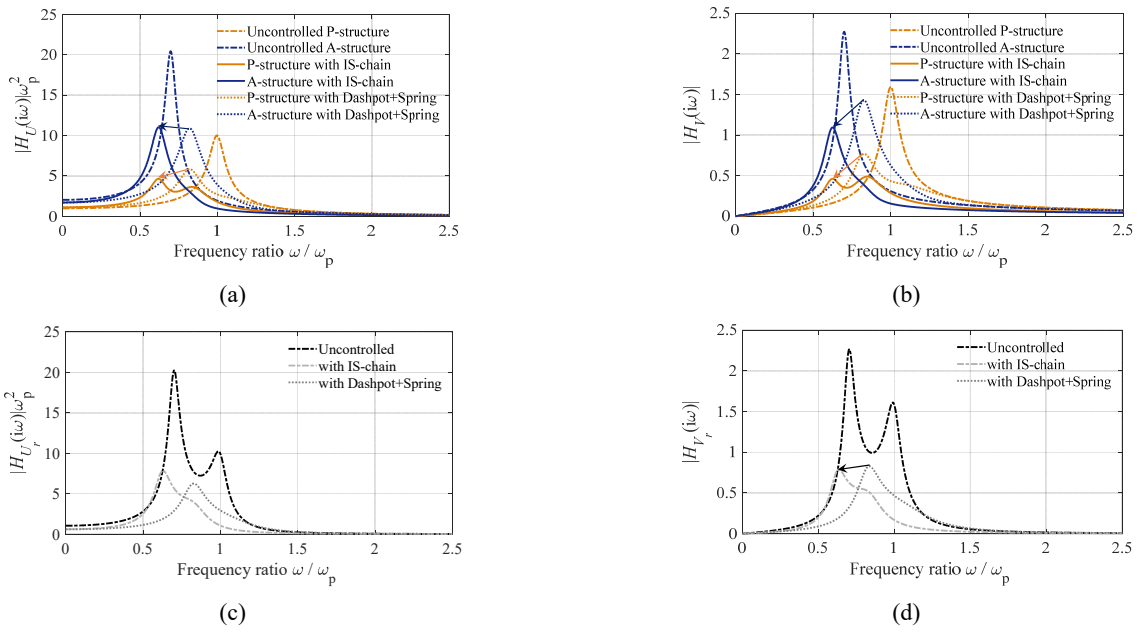

Fig. 7 Transfer function curves of displacement and velocity responses of the adjacent structures with inerter-system chain in Case B. (a) Displacement response $H_U(i\omega)$ of P- and A-structures; (b) velocity response $H_V(i\omega)$ of P- and A-structures; (c) $H_{U_r}(i\omega)$; and (b) $H_{V_r}(i\omega)$

μ. By the inspection of the optimized non-zero μ, the inter-placed inerter forming a complete inerter-chain is necessary to lighten the energy-dissipation burden imposed on the entire controlled structures.

Adopting the designed inerter-system chain in the stochastic response analysis, the control characteristic of the proposed inerter-system chain is the frequency domain, where the dashpot-spring system with the same parameters as the SDIS is analyzed for comparison. For Case B in Figs. 7(a)-(d), the inerter-system chain and the dashpot-spring system supply similar effectiveness for displacement reductions, while the former exhibiting lower velocity (energy) responses of the P-, A-structures, and the relative distance. A complete inerter chain facilitates the characteristic, including the tuning effect, the complete

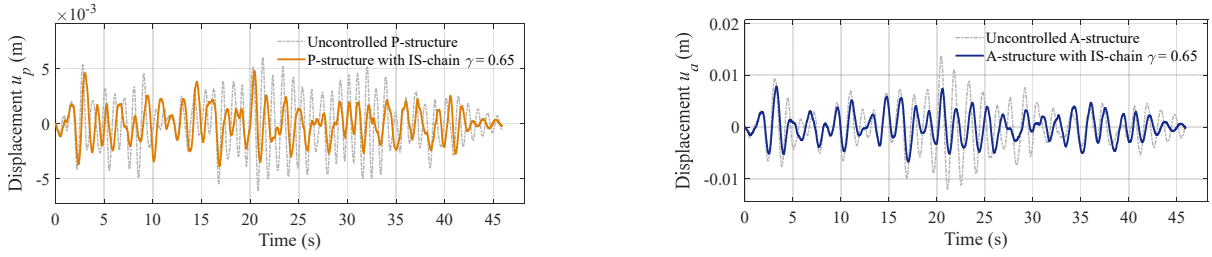

Fig. 8 Displacement responses of an uncontrolled structure and structure with an inerter-system chain for Case B ($\gamma_t = 0.65$) under the excitation of the white noise. (a) P-structure; and (b) A-structure

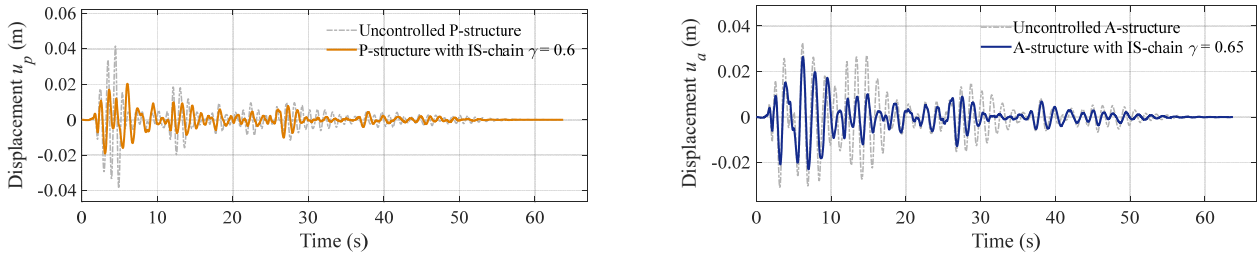

Fig. 9 Displacement responses of an uncontrolled structure and structure with an inerter-system chain for Case B ($\gamma_t = 0.65$) under the excitation of El Centro earthquake. (a) P-structure; and (b) A-structure

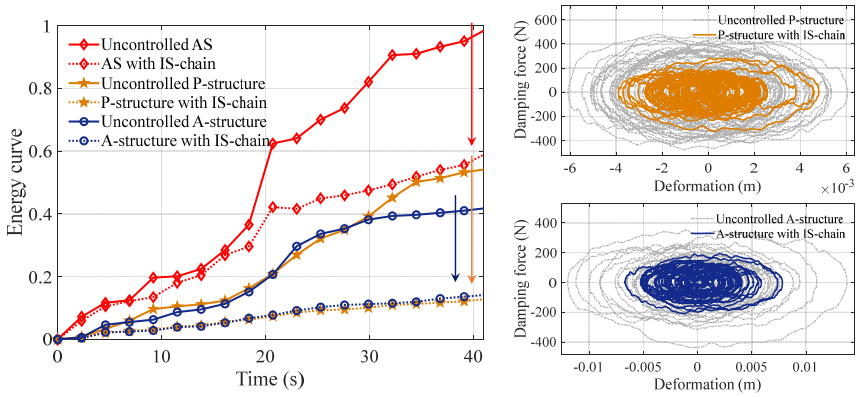

Fig. 10 Normalized energy curves and hysteretic curves of adjacent structures with and without an inerter-system chain under excitation of the white noise

entire adjacent structures. By the adjustment of the inertial possibility to improve the energy performance of the inerter-chain is preferred to suppress the peak response to avoid resonant vibrations shown as the two peaks of P- and A-structures in Figs. 7(a)-(b). For the distribution pattern in the frequency domain, the inerter-system chain is more effective in the resonant and high-frequency band, because of the implementation of an inter inerter.

To intuitively view the energy performances, the time history and energy-balance analyses were conducted for verification. Taking the white noise and the typical seismic ground motion from the El Centro earthquake as examples, the displacement, energy, and hysteretic curves are plotted in Fig. 8 to Fig. 10. The intensity measure of the excitation(for instance, the peak ground acceleration) does not affect the results in terms of vibration control ratios, under the assumption of the postulated linear behavior of the controlled systems. As highlighted by the displacement response ratio γ in the legend, the provided displacement performance matches the target demand. This indicates that the derived design formulae and developed design in Section 3 under the assumption of white-noise excitation can bring about a satisfactory performance for structures subject to real seismic excitations. Compared with uncontrolled adjacent structures, the inerter-system chain significantly reduces the entire input energy, with the less dissipated energy of the primary structures (marked by the arrows in Fig. 10). The reduced energy dissipation burden is also accompanied by the reduced deformation and saved damping force of primary structures.

5. Conclusions

This study proposed a novel configuration represented by adjacent structures coupled with an inerter-system chain that includes two end-placed inerter-dashpot dampers and one inter-placed SDIS. Stochastic energy balance establishes the theoretical basis of input-energy reduction principle for the developed inerter-based adjacent structures, successively yielding an energy-based design for the inerter-system chain. The main conclusions of this study can be drawn as follows:

- A complete inerter-system chain that composes three inerters in series exhibits a significant multi-reduction in the structural displacement, shear force, and dissipation energy burden. Particularly, the effectiveness of reducing the vibrational energy transmitted into the entire structures counts on the series inerter-chain, which differentiates the proposed chain from alternative layouts.
- Derived closed-form energy equation theoretically establishes the relationship between the input power, dissipation powers of adjacent structures and SDIS, and key parameters of the inerter-system chain in a quantitative manner. Revealed by the equation, the three inerters cooperated by the parallel spring adjust the distribution of the energy dissipation burdens among the damping elements in the considered system, which facilitates the minimization of the input power.
- Pursuing the energy-based advantageous features of the inerter-system chain, the proposed design framework is capable of minimizing the input energy that is equal to the total energy-based control cost, with target displacement-demand satisfied. This design method essentially supplies a proper approach to apply the proposed inerter-system chain for the reduced control force and energy dissipation demand.
- Validated by numerical examples, the analytical design equations derived on the zero-damping assumption can be applied to describe the optimized relationship between the key parameters of the SDIS. The obtained results of this study are based on the adjacent SDOF structures in a linear state. The application of the inerter-system chain can be extended into a more complex form for multi-degree of freedom structures with nonlinear behavior and will be studied in the future.

Acknowledgments

This study was supported by the National Natural Science Foundation of China (grant number 51778489 and

51978525), and the Basic Research Project of State Key Laboratory of Ministry of Science and Technology (grant number SLDRCE19A-02).

References

Arakaki, T., Kuroda, H., Arima, F., Inoue, Y. and Baba, K. (1999a), "Development of seismic devices applied to ball screw: Part 1 Basic performance test of RD-series", *J. Architect. Build. Sci.*, **5**(8), 239-244.

Arakaki, T., Kuroda, H., Arima, F., Inoue, Y. and Baba, K. (1999b), "Development of seismic devices applied to ball screw: Part 2 Performance test and evaluation of RD-series", *J. Architect. Build. Sci.*, **5**(9), 365-370.

Asai, T., Araki, Y. and Ikago, K. (2018), "Structural control with tuned inertial mass electromagnetic transducers", *Struct. Control Health Monitor.*, **25**(2), e2059. https://doi.org10.1002/stc.2059

Barredo, E., Blanco, A., Colín, J., Penagos, V.M., Abúndez, A., Vela, L.G., Meza, V., Cruz, R.H. and Mayén, J. (2018), "Closed-form solutions for the optimal design of inerter-based dynamic vibration absorbers", *Int. J. Mech. Sci.*, **144**, 41-53. https://doi.org/10.1016/j.ijmecsci.2018.05.025

Basili, M., De Angelis, M. and Pietrosanti, D. (2018), "Modal analysis and dynamic response of two adjacent single-degree-of-freedom systems linked by spring-dashpot-inerter elements", *Eng. Struct.*, **174**, 736-752. https://doi.org/10.1016/j.engstruct.2018.07.048

Bhaskararao, A.V. and Jangid, R.S. (2007), "Optimum viscous damper for connecting adjacent SDOF structures for harmonic and stationary white-noise random excitations", *Earthq. Eng. Struct. Dyn.*, **36**(4), 563-571. https://doi.org10.1002/eqe.636

Chen, M.Z.Q., Hu, Y., Li, C. and Chen, G. (2015), "Performance Benefits of Using Inerter in Semiactive Suspensions", *IEEE Transact. Control Syst. Technol.*, **23**(4), 1571-1577. http://dx.doi.org/10.1109/TCST.2014.2364954

Chen, Q.J., Zhao, Z.P., Zhang, R.F. and Pan, C. (2018), "Impact of soil–structure interaction on structures with inerter system", *J. Sound Vib.*, **433**, 1-15. https://doi.org/10.1016/j.jsv.2018.07.008

Chen, Q.J., Zhao, Z.P., Xia, Y.Y., Pan, C., Luo, H. and Zhang, R.F. (2019), "Comfort-based floor design employing tuned inerter mass system", *J. Sound Vib.*, **458**, 143-157. https://doi.org/10.1016/j.jsv.2019.06.019

Cimellaro, G.P. and Lopez-Garcia, D. (2011), "Algorithm for design of controlled motion of adjacent structures", *Struct. Control Health Monitor.*, **18**(2), 140-148. https://doi.org10.1002/stc.357

Crandall, S.H. and Mark, W.D. (2014), *Random Vibration in Mechanical System*, Academic Press.

De Domenico, D. and Ricciardi, G. (2018), "An enhanced base isolation system equipped with optimal tuned mass damper inerter (TMDI)", *Earthq. Eng. Struct. Dyn.*, **47**(5), 1169-1192. https://doi.org/10.1002/eqe.3011

De Domenico, D. and Ricciardi, G. (2019), "Earthquake protection of structures with nonlinear viscous dampers optimized through an energy-based stochastic approach", *Eng. Struct.*, **179**, 523-539. https://doi.org/10.1016/j.engstruct.2018.09.076

De Domenico, D., Deastra, P., Ricciardi, G., Sims, N.D. and Wagg, D.J. (2019a), "Novel fluid inerter based tuned mass dampers for optimised structural control of base-isolated buildings", *J. Franklin Inst.*, **356**(14), 7626-7649. https://doi.org/10.1016/j.jfranklin.2018.11.012

De Domenico, D., Ricciardi, G. and Takewaki, I. (2019b), "Design strategies of viscous dampers for seismic protection of building structures: A review", *Soil Dyn. Earthq. Eng.*, **118**, 144-165. https://doi.org/10.1016/j.soildyn.2018.12.024

De Domenico, D., Qiao, H., Wang, Q., Zhu, Z. and Marano, G. (2020), "Optimal design and seismic performance of Multi-Tuned Mass Damper Inerter (MTMDI) applied to adjacent high-rise buildings", *Struct. Des. Tall Special Build.*, **29**(14), e1781. https://doi.org/10.1002/tal.1781

Farghaly, A.A. (2015), "Seismic analysis of 3-D two adjacent buildings connected by viscous dampers with effect of underneath different soil kinds", *Smart Struct. Syst., Int. J.*, **15**(5), 1293-1309. https://doi.org/10.12989/sss.2015.15.5.1293

Greco, R. and Marano, G.C. (2016), "Multi-objective optimization of a dissipative connection for seismic protection of wall-frame structures", *Soil Dyn. Earthq. Eng.*, **87**, 151-163. https://doi.org/10.1016/j.soildyn.2016.01.020

Huang, Z., Hua, X., Chen, Z. and Niu, H. (2019), "Performance evaluation of inerter-based damping devices for structural vibration control of stay cables", *Smart Struct. Syst., Int. J.*, **23**(6), 615-626. https://doi.org/10.12989/sss.2019.23.6.615

Ikago, K., Saito, K. and Inoue, N. (2012), "Seismic control of single-degree-of-freedom structure using tuned viscous mass damper", *Earthq. Eng. Struct. Dyn.*, **41**(3), 453-474. http://dx.doi.org/10.1002/eqe.1138

Javidialesaadi, A. and Wierschem, N.E. (2019), "Energy transfer and passive control of single-degree-of-freedom structures using a one-directional rotational inertia viscous damper", *Eng. Struct.*, **196**, 12. http://doi.org/10.1016/j.engstruct.2019.109339

Jiang, Y.Y., Zhao, Z.P., Zhang, R.F., De Domenico, D. and Pan, C. (2020), "Optimal design based on analytical solution for storage tank with inerter isolation system", *Soil Dyn. Earthq. Eng.*, **129**, 105924. https://doi.org/10.1016/j.soildyn.2019.105924.

Kawamata, S. (1973), "Development of a vibration control system of structures by means of mass pumps", Institute of Industrial Science, University of Tokyo, Tokyo, Japan.

Kiureghian, A.D. and Neuenhofer, A. (1992), "Response spectrum method for multi-support seismic excitations", *Earthq. Eng. Struct. Dyn.*, **21**(8), 713-740. https://doi.org/10.1002/eqe.4290210805

Lazar, I.F., Neild, S.A. and Wagg, D.J. (2016), "Vibration suppression of cables using tuned inerter dampers", *Eng. Struct.*, **122**, 62-71. https://doi.org/10.1016/j.engstruct.2016.04.017

Marian, L. and Giaralis, A. (2014), "Optimal design of a novel tuned mass-damper–inerter (TMDI) passive vibration control configuration for stochastically support-excited structural systems", *Probabil. Eng. Mech.*, **38**, 156-164. https://doi.org/10.1016/j.probengmech.2014.03.007

Marian, L. and Giaralis, A. (2017), "The tuned mass-damper-inerter for harmonic vibrations suppression, attached mass reduction, and energy harvesting", *Smart Struct. Syst., Int. J.*, **19**(6), 665-678. https://doi.org/10.12989/sss.2017.19.6.665

Miari, M., Choong, K.K. and Jankowski, R. (2019), "Seismic pounding between adjacent buildings: Identification of parameters, soil interaction issues and mitigation measures", *Soil Dyn. Earthq. Eng.*, **121**, 135-150. https://doi.org/10.1016/j.soildyn.2019.02.024

Ng, C.L. and Xu, Y.L. (2006), "Seismic response control of a building complex utilizing passive friction damper: experimental investigation", *Earthq. Eng. Struct. Dyn.*, **35**(6), 657-677. https://doi.org/10.1002/eqe.549

Ok, S.Y., Song, J. and Park, K.S. (2008), "Optimal design of hysteretic dampers connecting adjacent structures using multi-objective genetic algorithm and stochastic linearization method", *Eng. Struct.*, **30**(5), 1240-1249. https://doi.org/10.1016/j.engstruct.2007.07.019

Palacios-Quiñonero, F., Rubió-Massegú, J., Rossell, J.M. and Karimi, H.R. (2019), "Design of inerter-based multi-actuator systems for vibration control of adjacent structures", *J. Franklin*

Inst., **356**(14), 7785-7809. https://doi.org/10.1016/j.jfranklin.2019.03.010

Reggio, A. and Angelis, M.D. (2015), "Optimal energy-based seismic design of non-conventional Tuned Mass Damper (TMD) implemented via inter-story isolation", *Earthq*. *Eng*. *Struct*. *Dyn*., **44**(10), 1623-1642. https://doi.org/10.1002/eqe.2548

Smith, M.C. (2002), "Synthesis of mechanical networks: the inerter", *IEEE Transact*. *Automat*. *Control*, **47**(10), 1648-1662. https://doi.org10.1109/TAC.2002.803532

Sugiura, K., Sawada, R., Nemoto, Y., Haraguchi, R. and Asai, T. (2020), "Wave flume testing of an oscillating-body wave energy converter with a tuned inerter", *Appl*. *Ocean Res*., **98**, 102127. https://doi.org/10.1016/j.apor.2020.102127

Takewaki, I., Murakami, S., Yoshitomi, S. and Tsuji, M. (2012), "Fundamental mechanism of earthquake response reduction in building structures with inertial dampers", *Struct*. *Control Health Monitor*., **19**(6), 590-608. http://dx.doi.org/10.1002/stc.457

Uang, C. and Bertero, V. (1988), "Use of energy as a design criterion in earthquake-resistant design", Technical Report UCB/EERC, Earthquake Engineering Research Center, University of California at Berkeley, CA, USA.

Wang, Q., Qiao, H., De Domenico, D., Zhu, Z. and Tang, Y. (2020), "Seismic response control of adjacent high-rise buildings linked by the Tuned Liquid Column Damper-Inerter (TLCDI)", *Eng*. *Struct*., **223**, 111169. https://doi.org/10.1016/j.engstruct.2020.111169

Xu, Y.L., Zhan, S., Ko, J.M. and Zhang, W.S. (1999), "Experimental investigation of adjacent buildings connected by fluid damper", *Earthq*. *Eng*. *Struct*. *Dyn*., **28**(6), 609-631. https://doi.org/10.1002/(sici)1096-9845(199906)28:6<609::aid-eqe831>3.0.co;2-s

Ying, Z.G., Ni, Y.Q. and Ko, J.M. (2003), "Stochastic optimal coupling-control of adjacent building structures", *Comput*. *Struct*., **81**(30), 2775-2787. https://doi.org/10.1016/S0045-7949(03)00332-8

Zhang, R.F., Zhao, Z.P. and Dai, K. (2019), "Seismic response mitigation of a wind turbine tower using a tuned parallel inerter mass system", *Eng*. *Struct*., **180**, 29-39. http://doi.org/10.1016/j.engstruct.2018.11.020

Zhang, R.F., Zhao, Z.P., Pan, C., Ikago, K. and Xue, S.T. (2020), "Damping enhancement principle of inerter system", *Struct*. *Control Health Monitor*., e2523. https://doi.org/10.1002/stc.2523

Zhao, Z.P., Zhang, R.F., Jiang, Y.Y. and Pan, C. (2019a), "Seismic response mitigation of structures with a friction pendulum inerter system", *Eng*. *Struct*., **193**, 110-120. https://doi.org/10.1016/j.engstruct.2019.05.024

Zhao, Z.P., Zhang, R.F., Jiang, Y.Y. and Pan, C. (2019b), "A tuned liquid inerter system for vibration control", *Int*. *J*. *Mech*. *Sci*., **164**, 105171. https://doi.org/10.1016/j.ijmecsci.2019.105171

Zhao, Z.P., Chen, Q.J., Zhang, R.F., Jiang, Y.Y. and Pan, C. (2020a), "A negative stiffness inerter system (NSIS) for earthquake protection purposes", *Smart Struct*. *Syst*., *Int*. *J*., **26**(4), 481-493. https://doi.org/10.12989/sss.2020.26.4.481

Zhao, Z.P., Chen, Q.J., Zhang, R.F., Pan, C. and Jiang, Y.Y. (2020b), "Energy dissipation mechanism of inerter systems", *Int*. *J*. *Mech*. *Sci*., **184**, 105845. https://doi.org/10.1016/j.ijmecsci.2020.105845